光学学报

携带横向轨道角动量的时空局域波包的传输特性（特邀）

张年佳[1]，曹前[1*]，Chong Andy[2]，詹其文[1]

[1]上海理工大学光电信息与计算机工程学院，上海 200093；

[2]釜山国立大学物理系，韩国 釜山 46241

摘要　光学轨道角动量（OAM）可以纵向OAM的形式存在于空间涡旋光束中，或以横向OAM的形式存在于时空光涡旋波包中。与涡旋光束不同，时空光涡旋波包在传播过程中同时受到衍射和色散效应的影响，造成波包在时空域内的展宽，并且时空光涡旋波包携带的横向OAM也会在传播过程中分裂。这两点限制了横向OAM在其他研究领域的应用。本文引入并研究了携带横向OAM的三维时空局域波包，此波包可以同时克服衍射与色散效应造成的时空域三维变化。在传播过程中，该时空局域波包的时空域分布不变，且在遇到障碍物后也能快速重新恢复到原有的状态，具有传播不变以及自恢复的特性。本文对时空局域波包的传播过程以及经过障碍物后的恢复过程进行了数值模拟仿真，证实了其传播不变特性和自恢复特性。这种携带横向OAM的三维时空局域波包为横向OAM未来的利用提供了新的机遇，有望应用于光通信、量子光学、光学成像等领域。

关键词　横向光学轨道角动量；三维时空局域波包；传播不变；自恢复

中图分类号　O436　　**文献标志码**　A　　**DOI**：10.3788/AOS231936

1　引　　言

从大气运动引发的飓风到水体流动产生的涡流，涡旋运动普遍存在于自然界中。Allen[1]在1992年发现涡旋光光场内的光子携带纵向轨道角动量（OAM）。这一发现为光学领域的研究提供了一个全新的可控维度，光学OAM被迅速应用于光通信、量子光学、超分辨成像、粒子捕获等领域[2-5]。已有的对光学OAM的研究集中于研究纵向OAM，即OAM方向平行于光场传播方向的涡旋光光场。而OAM方向可以是横向的，即OAM指向垂直于光场的传播方向。2005年，Sukhorukov等[6]从理论上证明了具有时空域涡旋相位的时空光涡旋（STOV）波包可以携带横向OAM；Jhajj等[7]在非线性脉冲自聚焦过程中成功生成并观察到了携带横向OAM的STOV波包；2020年，Chong等[8]利用线性光学器件生成了携带可控横向OAM的STOV波包。实验装置中利用到的时空光场整形系统也为横向OAM的研究提供了便捷的手段和重要的工具。最近，越来越多关于携带横向OAM的波包的研究被报道，包括在多个平面携带OAM的时空波包[9]、可以携带横向OAM和倾斜OAM的部分相干光源[10-11]、携带横向OAM的Airy脉冲[12]等，有望利用STOV进行图像检测[13]以及将STOV传入少模光纤中，验证了STOV在光纤中传播的可能性，为横向OAM通信提供了可能性[14]。

目前阻碍横向OAM利用的一大问题在于消除衍射和色散对时空光场演化的影响。以STOV为例，Huang等[15]发现在自由空间传播时，由于衍射和色散作用的不平衡，STOV会分裂成多个子波包，横向OAM的结构被破坏。而当衍射作用和色散作用达到平衡时，虽然横向OAM的结构在传播过程中得到保持，但是波包的尺寸会逐渐变大。为了克服这种现象，Cao等[16]提出利用时空贝塞尔光场加载时空涡旋相位，构成携带横向OAM的时空贝塞尔波包（BeSTOV），这种时空局域波包可以使横向OAM结构在较长距离内保持不变。但是BeSTOV的传播不变特性仅仅适用于BeSTOV所处的x-t平面，当受到y方向的扰动时，横向OAM的结构将被破坏。

本文提出了一类携带横向OAM的三维时空局域波包，这类波包具有时空域传播不变以及时空域自恢复特性。首先展示了携带纵向OAM与横向OAM的三维时空局域波包，以及两者之间的区别。随后计算

收稿日期：2023-12-15；**修回日期**：2024-01-17；**录用日期**：2024-01-21；**网络首发日期**：2024-02-20

基金项目：国家自然科学基金（92050202，12104309）、上海市科委“科技创新行动计划”扬帆计划（21YF1431500）

通信作者：*cao.qian@usst.edu.cn

了具有时空涡旋相位的三维时空局域波包携带的角动量数，证明其携带横向OAM的特性。最后利用数值模拟仿真，分别展示了三维时空局域波包所具有的传播不变以及自恢复特性。这些特性可以使光子横向OAM成为超快成像、光通信以及量子光学等研究领域的重要工具。

2　实验仿真与分析

2.1　携带横向OAM的三维时空局域波包

基于Mills等[17]提出的三维时空局域波包理论，具有球谐对称的三维时空局域波包的时空域分布可用角量子数 l 和拓扑荷数 m 进行表征。在渐变包络近似下，三维时空局域波包为亥姆霍兹方程的解：

$$-\mathrm{i}\frac{\partial\psi}{\partial z}=\frac{\partial^2\psi}{\partial x^2}+\frac{\partial^2\psi}{\partial y^2}+\frac{\partial^2\psi}{\partial t^2},\tag{1}$$

式中：ψ 为时空波包的复振幅分布；z 为纵向传播距离；x、y、t 为归一化空间坐标与时间坐标。在式(1)中，波包的传输介质具有负色散，这样 $\partial^2/\partial t^2$ 与拉普拉斯算子具有相同符号。在球坐标系 (R,θ,ϕ) 下，三维时空局域波包可写为

$$\psi=\sqrt{2\pi}\,\psi_0\mathrm{J}_l(\alpha R)P_l^m(\cos\theta)\exp(\mathrm{i}m\phi)\exp(-\mathrm{i}\alpha^2 z),\tag{2}$$

式中：ψ_0 是波包振幅；J_l 是球贝塞尔函数；P_l^m 是连带Legendre多项式；角量子数 l 和拓扑荷数 m 都是整数并且满足 $|m|\leqslant l$；α 是传播系数。在球坐标系下，ϕ 表示所选平面的螺旋相位，在以往的研究当中，螺旋相位被施加于 x-y 平面，此时局域波包可携带大小为 $m\hbar$ 的纵向OAM[18-20]。将极轴（t 轴）旋转 90°（y 轴），可以将螺旋相位施加于 x-t 平面。此时，三维时空局域波包将会携带大小为 $m\hbar$ 的横向OAM。

图1分别展示了当 $(l,m)=(2,1)$ 时，携带纵向OAM和横向OAM的时空局域波包三维强度分布：纵向OAM[图1(a)]和横向OAM[图1(b)]。在图1(a)中，螺旋相位存在于空间 x-y 平面中，极轴沿 t 方向上对齐。而在图1(b)中，涡旋相位存在于时空 x-t 平面中，极轴沿 y 方向上对齐。图1比较清楚地揭示了这两种局部波中的旋转关系，这种关系类似于传统的脉冲形式的涡旋光束和新型时空光涡旋（STOV）波包的区别。

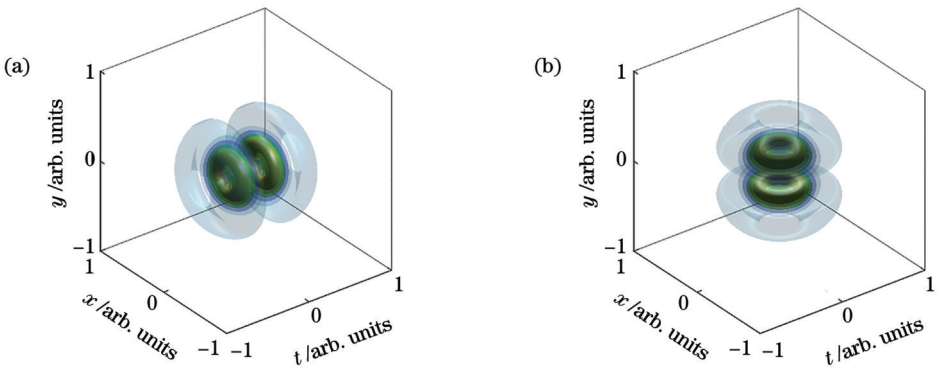

图1　携带纵向OAM和横向OAM的时空局域波包三维强度分布的比较。(a)携带纵向OAM的时空局域波包；(b)携带横向OAM的时空局域波包

Fig. 1　Comparison of 3D intensity distributions of two spatiotemporal localized wave packets with longitudinal OAM and transverse OAM. (a) Spatiotemporal localized wave packet with longitudinal OAM; (b) spatiotemporal localized wave packet with transverse OAM

不同于携带纵向OAM的涡旋光束[1]，时空光涡旋波包中的时空域涡旋相位 $\exp(\mathrm{i}l\phi_{x-t})$ 可使波包内的光子携带大小为 $m\hbar$ 的横向OAM[8]。式(2)中的螺旋相位项 ϕ 位于时空域中，它使波包能够携带横向OAM。为了研究这类波包的OAM密度[21-22]，需要分别计算波包的线动量密度 $\boldsymbol{g}$ 和角动量密度 $\boldsymbol{M}$。角动量密度 $\boldsymbol{M}$ 是位置矢量 $\boldsymbol{r}$ 和线动量密度 $\boldsymbol{g}$ 的叉乘积，写为

$$\boldsymbol{M}=\boldsymbol{r}\times\boldsymbol{g}。\tag{3}$$

电磁场所携带的线动量密度 $\boldsymbol{g}$ 可以表示为

$$\boldsymbol{g}=\frac{\varepsilon_0}{2}(E^*\times B+E\times B^*)=\frac{\varepsilon_0}{2}\left(c\frac{\partial u^*}{\partial x}\frac{\partial u}{\partial z}+\frac{\partial u}{\partial x}\frac{\partial u^*}{\partial z}+\mathrm{i}\omega u\frac{\partial u^*}{\partial x}-\mathrm{i}\omega u^*\frac{\partial u}{\partial x}\right)\hat{\boldsymbol{x}}+\frac{\varepsilon_0}{2}\left(\mathrm{i}\omega u\frac{\partial u^*}{\partial y}-\mathrm{i}\omega u^*\frac{\partial u}{\partial y}\right)\hat{\boldsymbol{y}}+$$
$$\frac{\varepsilon_0}{2}\left(\mathrm{i}\omega u\frac{\partial u^*}{\partial z}-\mathrm{i}\omega u^*\frac{\partial u}{\partial z}+2\omega k|u|^2\right)\hat{\boldsymbol{z}},\tag{4}$$

在柱坐标系下，式(4)可以改写为

$$\boldsymbol{g}=g_\rho\hat{\boldsymbol{\rho}}+g_\phi\hat{\boldsymbol{\phi}}+g_y\hat{\boldsymbol{y}}=$$
$$\frac{\varepsilon_0}{2}\left[\left(c\frac{\partial u^*}{\partial x}\frac{\partial u}{\partial z}+\frac{\partial u^*}{\partial x}\frac{\partial u}{\partial z}+i\omega u\frac{\partial u^*}{\partial x}-i\omega u^*\frac{\partial u}{\partial x}\right)\sin\phi+\left(i\omega u\frac{\partial u^*}{\partial z}-i\omega u^*\frac{\partial u}{\partial z}+2\omega k|u|^2\right)\cos\phi\right]\hat{\boldsymbol{\rho}}+$$
$$\frac{\varepsilon_0}{2}\left[\left(c\frac{\partial u^*}{\partial x}\frac{\partial u}{\partial z}+\frac{\partial u}{\partial x}\frac{\partial u^*}{\partial z}+i\omega u\frac{\partial u^*}{\partial x}-i\omega u^*\frac{\partial u}{\partial x}\right)\cos\phi-\left(i\omega u\frac{\partial u^*}{\partial z}-i\omega u^*\frac{\partial u}{\partial z}+2\omega k|u|^2\right)\sin\phi\right]\times$$
$$\left(i\omega u\frac{\partial u^*}{\partial z}-i\omega u^*\frac{\partial u}{\partial z}+2\omega k|u|^2\right)\hat{\boldsymbol{\phi}}+\frac{\varepsilon_0}{2}\left(i\omega u\frac{\partial u^*}{\partial y}-i\omega u^*\frac{\partial u}{\partial y}\right)\hat{\boldsymbol{y}},\tag{5}$$

式中：u是电磁场分布；ω是角频率。将式(2)代入式(5)，可以得到$g_y=0$，$\int_0^{2\pi}g_\rho\mathrm{d}\phi=0$以及$\int_0^{2\pi}g_\phi\mathrm{d}\phi=\frac{2\pi}{\rho}\varepsilon_0\omega|u|^2$。将计算出来的线动量密度代入式(3)，可计算出角动量密度。结果表明，在柱坐标系下时空局域波包存在沿y方向的角动量$\boldsymbol{M}=\boldsymbol{M}_y=\rho g_\phi\hat{\boldsymbol{y}}$，其他方向的角动量均为0。因此，每个光子携带的OAM可以由下式计算：

$$N_{\mathrm{OAM/photon}}=\frac{\int_{-\infty}^{\infty}M\mathrm{d}V}{\varepsilon_0\omega\int_{-\infty}^{\infty}|u|^2\mathrm{d}V}\hbar。\tag{6}$$

由式(6)可知，式(2)所描述的时空局域波包中每个光子所携带的横向OAM大小为$m\hbar$并且OAM的方向与传播轴z垂直。值得注意的是，由式(2)描述的时空局域波包具有无限能量，这种波包在物理上是不可能实现的。在实验中，可以使用高斯包络来截断理想的时空局域波包，则在$z=0$处的波包可表示为

$$\psi=\sqrt{2\pi}\,\psi_0\exp\left(-R^2/w^2\right)\mathrm{J}_l(\alpha R)P_l^m(\cos\theta)\times\exp(im\phi),\tag{7}$$

式中，w表征波包在球坐标下的尺寸。当w趋向于无穷时，式(7)描述了具有无穷能量的时空局域波包，这一类可携带横向OAM的三维时空局域波包如图2所示，图2(a)、2(b)、2(d)分别展示了不携带横向OAM的时空局域波包，当$(l,m)=(0,0)$时[图2(a)]，所得到的波包是一个球贝塞尔波包。

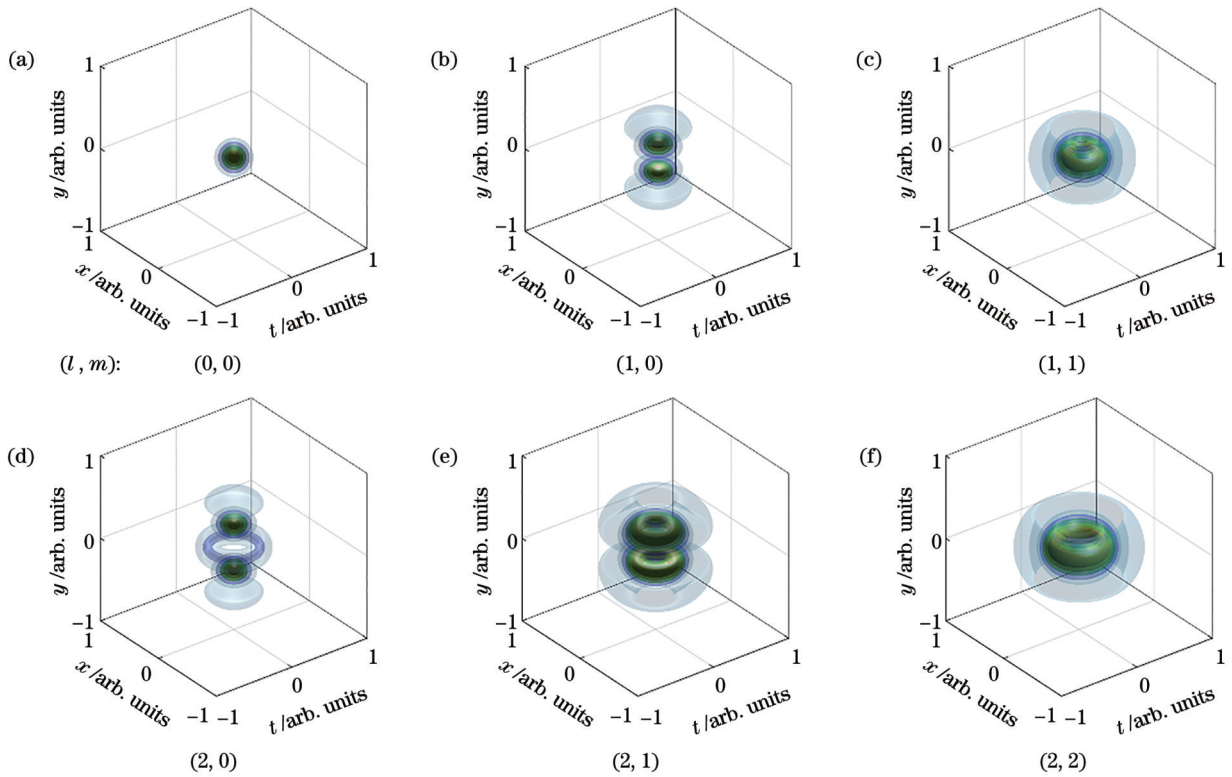

图2　携带和不携带横向OAM的时空局域波包的强度分布。(a)、(b)、(d)无横向OAM在不同角量子数下的波包强度分布；(c)、(e)、(f)携带高阶横向OAM的波包强度分布

Fig. 2　Intensity distributions of spatiotemporal localized wave packets without and with transverse OAM. (a), (b), (d) Intensity iso-surface without transverse OAM under different azimuthal quantum numbers; (c), (e), (f) intensity iso-surface with high-order transverse OAM

图 2(c)、2(e)、2(f)分别展示了携带不同横向OAM的时空局域波包。

2.2 携带横向OAM的三维时空局域波包的传播特性研究

为了研究携带横向OAM的时空局域波包的传播特性，对阶数$(l,m)=(2,1)$的时空波包在负色散介质中的传播演化进行了数值模拟仿真。时空局域波包具有的普遍特征是传播不变性，对于非时空局域波包而言，在传播过程中由于衍射和色散的共同作用，波包空间尺寸和时间尺寸会被拉伸。图 3 模拟了三维时空局域波包$(l,m)=(2,1)$在BK7玻璃中的传播演化，当波包的中心波长为1550 nm时，BK7材料的群速度色散(GVD)$\beta_2=-25.3\ \mathrm{fs^2/mm}$，满足时空局域波包的负色散要求。同时，时空局域波包的传播要求衍射作用和色散作用相同即等效衍射长度$L_{\mathrm{diff}}=\pi w_0^2/\lambda$和色散长度$L_{\mathrm{dis}}=\tau_0^2/\left|\beta_2\right|$相等，在$L=0$处，波包的脉冲宽度$\tau_0$和空间尺寸$w_0$分别设置为112.25 fs和0.30 mm。此时，$L_{\mathrm{diff}}=L_{\mathrm{dis}}=180$ mm，衍射长度和色散长度相等。图 3(a)～(d)为时空局域波包分别在传播距离$L=0$、$L=3L_{\mathrm{diff}}$、$L=6L_{\mathrm{diff}}$以及$L=9L_{\mathrm{diff}}$下三维强度图以及在x-t平面的投影强度图。图 3 表明，携带横向OAM的时空局域波包即便在$L=9L_{\mathrm{diff}}$的传播距离下，依旧保持其强度形状，没有发生任何明显的畸变或者扭曲。

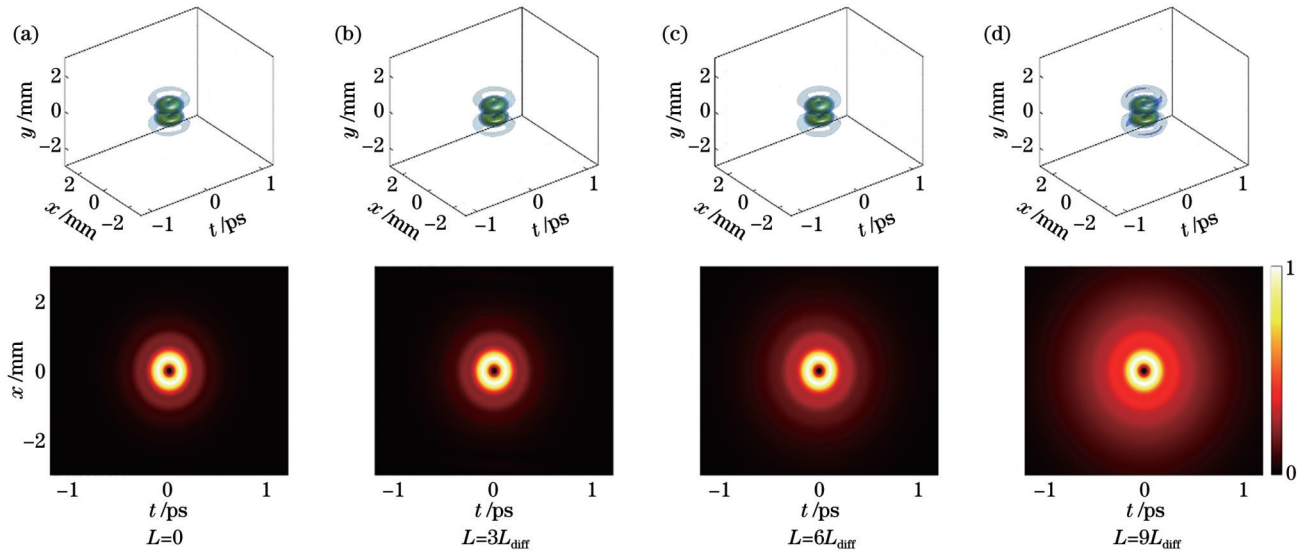

图 3　携带横向OAM的时空局域波包的传播不变特性数值仿真。(a)～(d)$(l,m)=(2,1)$的波包在不同传播距离下的三维强度图以及二维平面强度图。(a) 0；(b) $3L_{\mathrm{diff}}$；(c) $6L_{\mathrm{diff}}$；(d) $9L_{\mathrm{diff}}$

Fig. 3　Numerical simulation of invariant propagation of spatiotemporal localized wave packet with transverse OAM. 3D intensity map and 2D planar intensity map of wave packet with $(l,m)=(2,1)$ at (a) 0; (b) $3L_{\mathrm{diff}}$; (c) $6L_{\mathrm{diff}}$; (d) $9L_{\mathrm{diff}}$

图 3 表明了时空局域波包在传播过程中保持不变。为了说明更加充分，模拟了非时空局域波包在同等条件下的传播演化。取时空局域波包(2,1)的主瓣，如图 4(a)所示，在同样色散介质下传播，可以发现在$L=6L_{\mathrm{diff}}$时，时空局域波包的三维强度图以及投影图没有明显的变化，但是非局域时空波包的空间尺寸和时间尺寸迅速扩大。图 4 表明一个携带了横向OAM的波包在传播过程中尺寸不断变大，这可能会限制横向OAM在长距离通信方面的应用，而相比于普通时空波包，携带横向OAM的时空局域波包在更长的传播距离内实现尺寸不变，弥补了这一缺陷。图 3 和图 4 共同说明了本文所提出的三维时空局域波包具有传播不变特性。

但是，只有当衍射效应和色散效应相互平衡时，波包才具有局域特性，换句话说，不平衡的衍射和色散的条件下，波包不再具有传播不变的特性。此外，虽然波包能量有限，波包的局域特性不能够得到永久保持，但是，此时的传播不变长度要远远大于非局域时空波包的传播距离。

另一方面，时空局域波包具有自恢复的功能，可以实现在障碍物后的波包重建。为了验证时空局域波包的自恢复特性，本文模拟时空局域波包通过一个完全吸收电磁场的矩形板(宽度约为600 μm)，并在BK7($\beta_2=-25.26\ \mathrm{fs^2/mm}$)玻璃中传播遮挡后的波包。图 5(a)～(d)显示了在负色散介质中遮挡波包在不同传播长度(0、230、320、500 mm)的三维强度分布图。可以看到，在图 5(b)～(c)中上遮挡区域和下遮挡区域分成两个圆环，并向中心部分移动。最后，波包可以恢复到图 5(d)中原始的时空局域波包。遮挡波包在y-t平面上不同传播距离下的线性动量密度和强度分布如图 5(e)～(h)所示，揭示了自恢复过程中波包能流的分布。由于实际的传播环境都是三维的，当受到三维扰

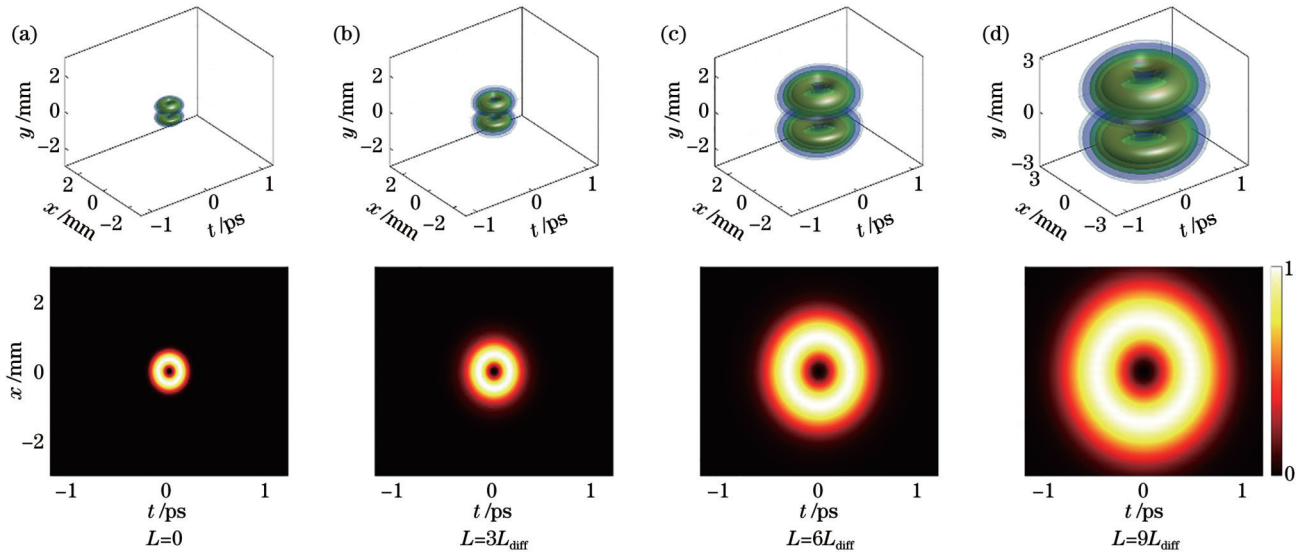

图4　携带横向OAM的非时空局域波包的传播特性数值仿真。(a)～(d)非局域时空波包在不同传播距离下的三维强度图以及二维平面强度图。(a) 0;(b) $3L_{\mathrm{diff}}$;(c) $6L_{\mathrm{diff}}$;(d) $9L_{\mathrm{diff}}$

Fig. 4　Numerical simulation of propagation characteristics of non spatiotemporal localized wave packet with transverse OAM. 3D intensity map and 2D planar intensity map of non spatiotemporal localized wave packet at (a) 0; (b) $3L_{\mathrm{diff}}$; (c) $6L_{\mathrm{diff}}$; (d) $9L_{\mathrm{diff}}$

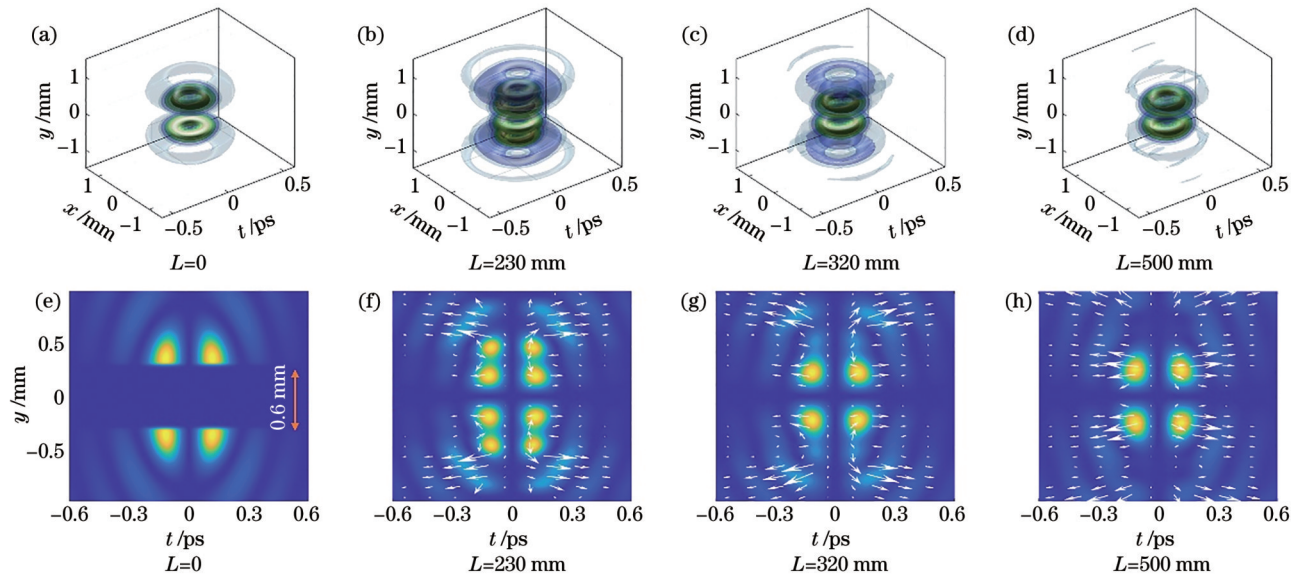

图5　时空局域波包$(l,m)=(2,1)$的自恢复演化过程。(a)～(d)时空局域波包的三维强度演化;(e)～(h)时空局域波包在y-t平面不同位置处的二维能流分布演化

Fig. 5　Self-healing process of spatiotemporal localized wave packet with $(l,m)=(2,1)$. (a)–(d) 3D intensity evolution of spatiotemporal localized wave packet; (e)–(h) evolution of 2D energy flow distribution of spatiotemporal localized wave packet at different positions in y-t plane

动破坏了波包结构后,对于传统的二维时空局域波包来说,无法实现自恢复,但是本文提出的三维时空局域波包可以重新恢复波包结构,抗扰动能力强,有望应用于光通信、成像等领域。

3　结　　论

综上所述,本文提出了一类新型的携带横向OAM的三维时空局域波包,并利用数值模拟仿真结果证明了这类波包的传播不变及自恢复特性。这类波包的横向OAM结构可以在长传播距离下(9倍等效衍射距离/色散距离)维持其时空域三维分布,克服了STOV在自由空间传播时的波包分裂现象或者波包尺寸展宽的问题。此外,该波包可以在遭遇三维障碍物后实现波包在时空域内的重建。这些特性是传统的二维时空局域波包不具备的。

近年来,人们对横向OAM的研究越来越多,对横

向OAM的应用领域也在不断进行探索。本文提出的将横向OAM结构嵌入至时空局域波包的方法，可以克服横向OAM在传播过程中所发生的畸变，对于横向OAM的利用有着重要意义，有望应用于超快成像、光通信以及量子光学等领域。

参 考 文 献

[1] Allen L, Beijersbergen M W, Spreeuw R J, et al. Orbital angular momentum of light and the transformation of Laguerre-Gaussian laser modes[J]. Physical Review A, 1992, 45(11): 8185-8189.

[2] Zhao Y F, Liu J, Li S H, et al. Secure optical interconnects using orbital angular momentum beams multiplexing/multicasting[J]. Advanced Photonics Nexus, 2023, 3(1): 016004.

[3] Gabriel C, Aiello A, Zhong W, et al. Entangling different degrees of freedom by quadrature squeezing cylindrically polarized modes[J]. Physical Review Letters, 2011, 106(6): 060502.

[4] 王佳林, 严伟, 张佳, 等. 受激辐射损耗超分辨显微成像系统研究的新进展[J]. 物理学报, 2020, 69(10): 108702.
Wang J L, Yan W, Zhang J, et al. New advances in the research of stimulated emission depletion super-resolution microscopy[J]. Acta Physica Sinica, 2020, 69(10): 108702.

[5] Padgett M, Bowman R. Tweezers with a twist[J]. Nature Photonics, 2011, 5: 343-348.

[6] Yangirova V V, Sukhorukov A P. Spatio-temporal vortices: properties, generation and recording[C]//EQEC '05. European Quantum Electronics Conference, June 12-17, 2005, Munich, Germany. New York: IEEE Press, 2005: 93.

[7] Jhajj N, Larkin I, Rosenthal E W, et al. Spatiotemporal optical vortices[J]. Physical Review X, 2016, 6(3): 031037.

[8] Chong A, Wan C H, Chen J, et al. Generation of spatiotemporal optical vortices with controllable transverse orbital angular momentum[J]. Nature Photonics, 2020, 14: 350-354.

[9] Gu L L, Cao Q, Zhan Q W. Spatiotemporal optical vortex wavepackets with phase singularities embedded in multiple domains[J]. Chinese Optics Letters, 2023, 21(8): 080003.

[10] Mirando A, Zang Y M, Zhan Q W, et al. Generation of spatiotemporal optical vortices with partial temporal coherence [J]. Optics Express, 2021, 29(19): 30426-30435.

[11] Adams J, Chong A. Tilted spatiotemporal optical vortex with partial temporal coherence[J]. Chinese Optics Letters, 2023, 21(12): 120002.

[12] Zang Y M, Wei F L, Kim H S, et al. Temporal manipulation of spatiotemporal optical vortices with an Airy pulse[J]. Chinese Optics Letters, 2023, 21(8): 080002.

[13] Huang J Y, Zhang J H, Zhu T F, et al. Spatiotemporal differentiators generating optical vortices with transverse orbital angular momentum and detecting sharp change of pulse envelope [J]. Laser & Photonics Reviews, 2022, 16(5): 2100357.

[14] Cao Q, Chen Z, Zhang C, et al. Propagation of transverse photonic orbital angular momentum through few-mode fiber[J]. Advanced Photonics, 2023, 5(3): 036002. [LinkOut]

[15] Huang S L, Wang P, Shen X, et al. Diffraction properties of light with transverse orbital angular momentum[J]. Optica, 2022, 9(5): 469-472.

[16] Cao Q, Chen J, Lu K Y, et al. Non-spreading Bessel spatiotemporal optical vortices[J]. Science Bulletin, 2022, 67(2): 133-140.

[17] Mills M S, Siviloglou G A, Efremidis N, et al. Localized waves with spherical harmonic symmetries[J]. Physical Review A, 2012, 86(6): 063811.

[18] Vasara A, Turunen J, Friberg A T. Realization of general nondiffracting beams with computer-generated holograms[J]. Journal of the Optical Society of America A, 1989, 6(11): 1748-1754.

[19] Li H, Huang X, Cao Q, et al. Generation of three-dimensional versatile vortex linear light bullets[J]. Chinese Optics Letters, 2017, 15(3): 030009.

[20] López-Ripa M, Sola Í J, Alonso B. Bulk lateral shearing interferometry for spatiotemporal study of time-varying ultrashort optical vortices[J]. Photonics Research, 2022, 10(4): 922-931.

[21] Wan C H, Chen J, Chong A, et al. Photonic orbital angular momentum with controllable orientation[J]. National Science Review, 2021, 9(7): nwab149.

[22] Lotti A, Couairon A, Faccio D, et al. Energy-flux characterization of conical and space-time coupled wave packets [J]. Physical Review A, 2010, 81(2): 023810.

Propagation Dynamics of Spatiotemporal Localized Wave Packets Carrying Transverse Orbital Angular Momentum (Invited)

Zhang Nianjia[1], Cao Qian[1*], Chong Andy[2], Zhan Qiwen[1]

[1]*School of Optical-Electrical and Computer Engineering, University of Shanghai for Science and Technology, Shanghai* 200093, *China*;

[2]*Physics Department, Pusan National University, Busan* 46241, *Republic of Korea*

Abstract

Objective The optical orbital angular momentum (OAM) can exist either as longitudinal OAM in the spatial vortex beam or transverse OAM in the spatiotemporal optical vortices. In contrast to the amount of research focused on longitudinal OAM, very few pay attention to optical fields with transverse OAM. Unlike longitudinal OAM which is only affected by diffraction, transverse OAM can be affected by both diffractive effect and dispersive effect. One of the biggest challenges in utilizing optical fields carrying transverse OAM is to overcome diffraction and dispersion as the optical field propagates.

Diffraction and dispersion will cause the fields to spread in space and time, which limits the applications of the optical field with OAM. We introduce a class of three-dimensional (3D) spatiotemporal localized wave packets with transverse optical OAM. The combination of the transverse OAM and the localized waves enables it to be immune to both dispersion and diffraction as the wave packet propagates. 3D spatiotemporal localized wave packets carrying transverse OAM provide a new opportunity for the utilization of transverse OAM and are expected to be applied in optical communication, quantum optics, and other fields in the future.

Methods In previous studies, the vortex phase is placed in the spatial x-y plane and the resulting localized wave packet carries longitudinal OAM. In this study, we rotate the polar axis by 90°, so that it is now aligned in the y-direction. Therefore, the vortex phase term $e^{im\phi}$ locates in the x-t plane. Two spatiotemporal localized wave packets carrying two types of OAM: longitudinal OAM and transverse OAM are plotted (Fig. 1). Then, the theoretical derivation [Eqs. (4)–(6)] proves that the transverse OAM possessed by each photon is $m\hbar$. In Fig. 2, 3D spatiotemporal localized wave packets described by Eq. (7) with different orders are presented. From the basic-order to higher-order 3D spatiotemporal localized wave packets with transverse OAM, a kind of 3D spatiotemporal localized wave packets in abnormal medium is proposed.

Results and Discussions To investigate the localized property, we choose one of the family of 3D localized wave packets and simulate its propagation in a virtual medium BK7 with negative material dispersion ($\beta_2 = -25.26$ fs^2 mm^{-1}) at the central wavelength of 1550 nm. As a comparison, we filter out the central lobe of the wave packet and propagate it in the same medium. Due to the condition that the effects of diffraction and dispersion are equalized, a proper pulse duration and beam size of the filtered wave packet is 112.25 fs and 0.30 mm at $L=0$ mm, respectively. Hence, we have diffractive length and dispersive length around $L_{\mathrm{diff}} = L_{\mathrm{dis}} = 180$ mm. As shown in Figs. 3 and 4, the spatiotemporal localized wave packet keeps its intensity shape without any distorts during propagation. It is noted that the central lobe wave packet experiences dramatic change and is magnified proportionally in intensity profile compared with the spatiotemporal localized wave packet. The propagation invariability of spatiotemporal localized wave packets has been presented. The ability of the wave packet to propagate free of diffraction/dispersion is only valid when the diffraction effect and the dispersion effect are balanced with each other. In other words, the wave packets propagate unstably in the unbalanced diffraction and dispersion. In addition, the localized capacity cannot be continued permanently due to finite energy in practice. However, the limited invariantly propagated length is longer than the length of the filtered wave packets. On the other side, self-healing is also often used to characterize non-spreading wave packets, leading to a wavefront reconstruction after an electromagnetic absorption obstacle. To verify the self-healing of the spatiotemporal localized waves, we numerically simulate that a rectangular plate (around widths of 600 μm) perfectly absorbing electromagnetic fields is placed in the central part of the spatiotemporal localized wave packet and propagate the blocked wave in BK7 ($\beta_2 = -25.26$ fs^2 mm^{-1}). 3D iso-intensity profile of the blocked wave packet in anomalous medium at different propagated lengths (0, 230, 320, and 500 mm) is shown in Fig. 5. We can see that the up blocked area and the down area are split into two rings and move towards to the central part in Fig. 5(d). In the end, the wave packets can be recovered to their original spatiotemporal localized wave packets. The linear momentum density and intensity distribution of the blocked wave packet at different propagated distances in y-t plane are shown in Figs. 5(e)–5(h). The direction of linear momentum density is labelled by arrows and points to the blocked areas visually indicating the reason why self-healing can happen in the spatiotemporal localized wave packets.

Conclusions In summary, we present a new class of 3D spatiotemporal localized wave packets carrying transverse optical OAM. These wave packets exist in abnormal dispersion and can propagate invariantly when the diffractive effect and the dispersive effect are equal. To investigate the non-spreading nature of these wave packets, we simulate a wave packet $(l, m) = (2, 1)$ propagating in a proper and real medium BK7 glass. The results show that the wave packet propagates over several Rayleigh lengths while keeping its structure invariant. The wave packet can be recovered to its origin even when passing through a blocked obstacle. This kind of wave packets may provide new applications related to transverse OAM in the fields such as quantum optics and optical communications.

Key words transverse optical orbital angular momentum; three-dimensional spatiotemporal localized wave packet; invariant propagation; self-healing